Noise-induced quasiperiod and period switching

Yuxuan Wu,[1] Yuxing Jiao,[1] Yanzhen Zhao,[2] Haojun Jia,[3] and Liufang Xu[1,*]

[1]*Biophysics & Complex System Center, Center of Theoretical Physics, College of Physics, Jilin University Changchun 130012, People's Republic of China*

[2]*Department of Physics, Applied Physics and Astronomy, Rensselaer Polytechnic Institute, Troy, New York 12180, USA*

[3]*Department of Chemistry, Massachusetts Institute of Technology, Cambridge, Massachusetts 02139, USA*

(Received 29 June 2021; revised 25 October 2021; accepted 3 January 2022; published 31 January 2022)

We employ a typical genetic circuit model to explore how noise can influence dynamic structure. With the increase of a key interactive parameter, the model will deterministically go through two bifurcations and three dynamic structure regions. We find that a quasiperiodic component, which is not allowed by deterministic dynamics, will be generated by noise inducing in the first two regions, and this quasiperiod will be more and more stable along with the increase in noise. In particular, in the second region the quasiperiod will compete with a stable limit cycle and perform a new transient rhythm. Furthermore, we ascertain the entropy production rate and the heat dissipation rate, and discover a minimal value with theoretical elucidation. In the end, we unveil the mechanism of the formation of quasiperiods, and show a practical biological example. We expect this work to be helpful in solving some biological or ecological problems, such as the genetic origin of periodical cicadas and population dynamics with fluctuation.

DOI: 10.1103/PhysRevE.105.014419

I. INTRODUCTION

The periodicity of life has always been a fascinating issue. This periodicity is often realized by a set of genetic circuits, which are ubiquitous in life. Many important biological functions, such as circadian rhythms of mammals and some unicellular organisms [1–3], cell cycle processes of bacteria [4], oscillators in *Xenopus* embryonic cells [5], etc., are regulated by a genetic circuit containing positive and negative feedback. The essence of the genetic circuit is some interrelated biochemical reactions, which can be described by a set of differential equations.

However, the biosystem cannot be simulated only by deterministic dynamics, because noise is inevitable—even a natural and indispensable part of biological systems, having caused a lot of interesting phenomena, for instance, the regulation of the noise effect in eukaryotic gene expression [6], the stochastic focusing phenomenon [7], the influence of noise in *Bacillus subtilis* cells [8], the positive roles in plant cells [9], and many other discoveries [5,10–15]. Noise can also have the more counterintuitive effect of generating new stable states that do not exist in the absence of fluctuations, and most of the existing works focus on the two-state transition induced by noise [16–20]. This transition requires the bistable structure of the system. Further, it is of practical significance to explore whether random action can produce near-stable periodic oscillation, regarding which there have been some theoretical efforts on this matter [21,22]. If so, what kind of new system will be formed by the new periodic behavior and the original system? What will happen to its nature? Hitherto, definitive answers to these questions have been scarce.

Our work takes a concrete model as the starting point and endeavors to answer the above questions, the model of which was first proposed in the literature [23]. It is a typical genetic circuit structure with positive and negative feedback, which often appears in various biological systems (in some cases as a part of the system) [4,24]. We elaborate upon it in the section where we introduce the model, and show its detailed dynamic properties, as well as an undiscovered Hopf bifurcation point, which leads to the emergence of a stable limit cycle state. By changing a key parameter, the system will experience three different dynamic structures. A quasiperiodic dynamic state induced by noise appears in two of the three dynamic structures. In particular, it is impossible for this periodic structure to exist according to deterministic dynamics.

With the help of the theory of generalized potential and probability flow [25,26], we show the dynamic structure of the system in the form of the probability distribution, and the motion trend of the state points representing the position of the system in the phase space. It can be confirmed that the above two aspects support each other by the analysis of the trajectory of the state point in the noise environment. Next, we define the barrier height and the average first passage time; the former can quantify the ability of the system to form a periodicity, and the latter can effectively measure the cycle length of this periodicity. We have also clarified the relationship between the two. In particular, we give a practical biological example and make a brief analysis to show the possible universality of this noise-induced periodicity in biology.

As a nonequilibrium system, it will exchange energy with the outside environment and generate dissipation. The cost of dissipation is likely to be related to the stability of the

*lfxuphy@jlu.edu.cn

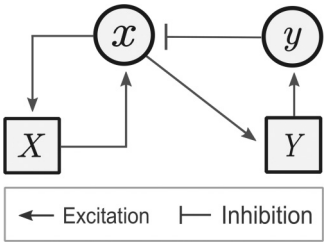

FIG. 1. Illustration of the model of an activator-repressor circuit.

system, which is also of interest to us; that is, under what conditions is the noise-induced quasiperiodic structure most stable? The answer to this question is important for us to understand and utilize this quasiperiodic structure. Therefore, we study the entropy production rate and the associated heat dissipation rate. In general, due to the nonequilibrium nature of biological systems, the entropy generation rate is a more common physical quantity in related research [27–29]. Indeed, the determination of the entropy production rate plays a decisive role in active particles [30,31], single-cell biological systems [32], soft biological materials [33], complex networks [34], and so on. Equally, the concomitant heat dissipation rate is also an important physical quantity [35–39]. When describing the global properties of the nonequilibrium system, they are like two sides of a coin. Some studies also show that the entropy production rate and heat dissipation rate are intimately related to the robustness of the system [40–42].

We offer an interpretation for the physical significance of the minimal value we found in the research of the heat dissipation rate. One can see the Supplemental Material (SM) for proof for consolidating the physical significance we interpret, and an interesting intuitive result [43].

II. MODEL

A. Structure determined by nonlinear dynamics and the changes in topology

In this work, the model is a simple activator-repressor circuit [23]; see Fig. 1. For a biosystem, x and y are two products (activator protein and repressor protein), and X, Y are the corresponding genes. x has a self-excited subcircuit, while y is excited by x, which in turn inhibits x. x and y are major research objects in our work, for the reason that X and Y can be eliminated adiabatically. This is because the dynamics of mRNA transcribed by corresponding genes represented by X and Y is much faster than that of the proteins represented by x and y [23].

Eventually, the model can be simplistically described by a set of two-dimensional equations as

$$\frac{dx}{dt} = F_1(x,y) = \alpha_1 + \frac{\beta_1 x^n}{k_1^n + x^n} - \delta xy - \lambda_1 x, \tag{1}$$

$$\frac{dy}{dt} = F_2(x,y) = \alpha_2 + \frac{\beta_2 x^p}{k_2^p + x^p} - \lambda_2 y. \tag{2}$$

One can see details of the coefficients in F_1 and F_2 in the Appendix. This set of equations describes the dynamic behavior of a biological system in phase space. In this model, the change of dynamic properties and topological structure

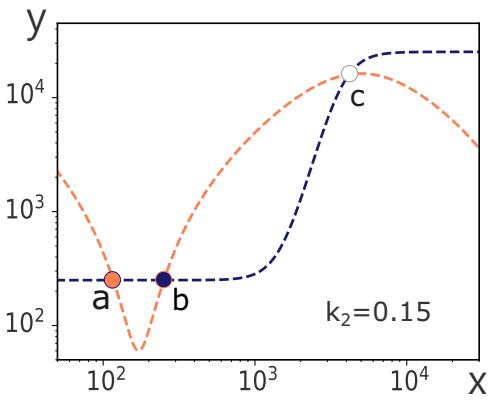

FIG. 2. Nullclines of x and y, and their intersection. $k_2 = 0.15$ is selected as a sample. The orange dashed line depicts x nullcline, and blue for y. Intersection depicted by the solid circle filled with orange (a) is a stable node, solid circle filled with blue (b) for the saddle, and open circle (c) for focus. In the range $k_2 \in [0.12, 0.17]$, the system will maintain this structure.

is obtained by changing k_2. We focus on the kinetic behavior in the first quadrant. In the range $k_2 \in [0.12, 0.17]$, nullclines of x and y have three intersection points, and two bifurcation points of the dynamics structure (C1 and C2) were found, as shown in Figs. 2 and 3. The reason why we choose the range $k_2 \in [0.12, 0.17]$ is that it is symmetric to the two bifurcation points which have a critical influence on the structure of the system, and the system will maintain the corresponding structure outside this range. The stability of those three intersections can be determined by discriminants. One of those two bifurcation points (C2), $k_2 = 0.1559$, can be determined by solving nullclines ($F_1 = 0$ and $F_2 = 0$) with discriminant of focus simultaneously. Another one (C1), $k_2 \in (0.1474, 0.1475)$, which is a *saddle-node-separatrix-loop* (SNL) bifurcation [44], was found by simulation but not by analysis. One can see details about solving the bifurcation in the SM [43]. What should be emphasized is that we found a stable limit cycle around the unstable focus in the range $k_2 \in [0.1475, 0.1559)$.

Bifurcation of the system means the changes of topological structure [45]. In nonlinear dynamics, we consider it as the phase transition of the system. Stable and unstable manifolds are streamlines starting from or going back to the saddle. Therefore, we can judge and predict the behavioral trend of every streamline by considering the shape of the nullclines together with the manifolds. Markedly, there is a bifurcation (C1) on the number axis between $k_2 = 0.1474$ and $k_2 = 0.1475$, on each side of which the structure of the system is essentially different from the structure on another side (Figs. S5(d), S5(e), S5(d1), and S5(e1) in the SM [43]). Figures S5(f) and S5(f1) in the SM show a Hopf bifurcation at $k_2 = 0.1559$ (C2) [43]. From the right to the left of C2 on the number axis, a stable focus develops into the stable limit cycle, which is the typical characteristic of Hopf bifurcation.

In the following, we sum up the global kinetic properties determined by deterministic nonlinear dynamics in the first quadrant:

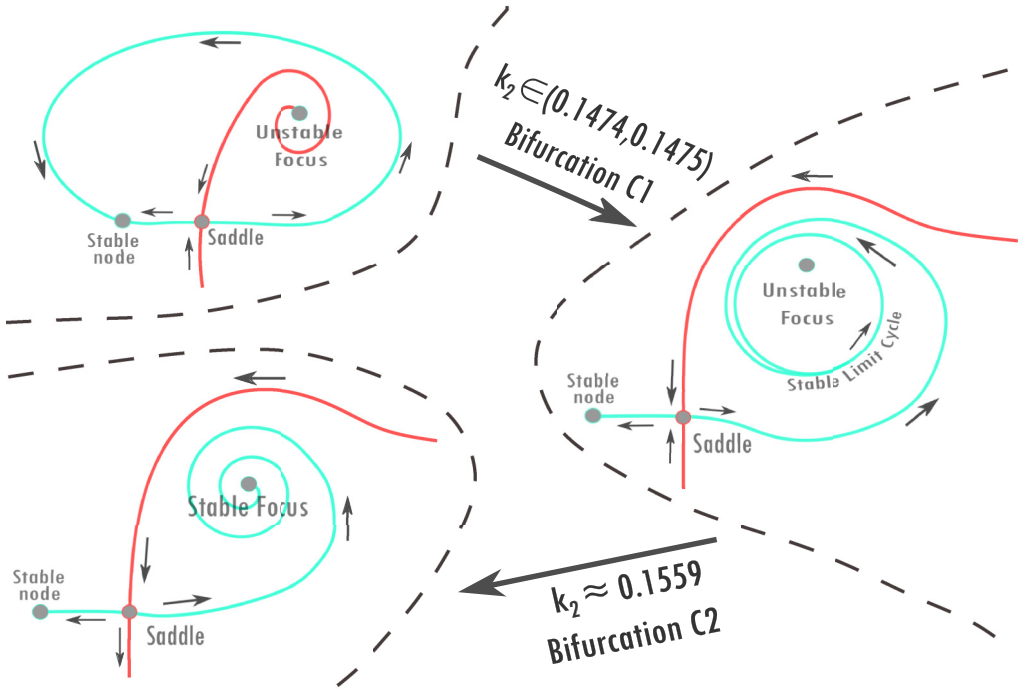

FIG. 3. Summary illustration of the topological structure's change. Crimson solid lines depict the stable manifolds and cyan solid lines depict unstable manifolds, and trends of manifolds are marked by arrows. As k_2 crosses C1, the stable manifold is peeled off from the focus, and a node that started at the stable node strides over the part between the stable node and the saddle. Meanwhile, there is a stable limit cycle formed. After k_2 crosses C2, the limit cycle shrinks to the focus. It is like a donut turning into a mug.

Parameter interval I, $k_2 \in [0.12, 1474]$. The system has a stable node in the left-bottom part nearby the saddle, which is the only stationary structure of the system. An unstable manifold forms a large closed loop, by which the unstable focus is encircled. That hints that our system can form a loop if the state point of the system at the left-bottom node strides across the saddle.

Parameter interval II, $k_2 \in (0.1559, 0.17]$. The whole region is divided into two parts by a stable manifold back to the saddle, in each of which there is a stationary structure, being the stable focus and the stable node. In the area where the stable node is located, every state point will return to the stable node. Similarly, state points will return to the stable focus in another area.

Parameter interval III, $k_2 \in (0.1475, 0.1559)$. The whole region is divided into two parts by a stable manifold similar to what we see in parameter interval II, in each of which there is a stationary structure, being the limit cycle and the node. If k_2 is close to the right neighborhood of C1, the limit cycle will cling to the stable manifold, being a large loop, which is similar to that in parameter interval I. If k_2 is close to the left neighborhood of C2, the limit cycle will tightly surround the unstable focus in the neighborhood of the focus, which is similar to that in parameter interval II.

B. Stochastic dynamics model

We construct a stochastic dynamic model by adding white noise to the deterministic nonlinear dynamic system, for the reason that white noise is a good approximation to the actual situation, and this simple noise is very representative [46], having played an important role in many studies [26,47–50]. The stochastic differential equations (SDEs) derived from Eqs. (1) and (2) are written as

$$\frac{dx}{dt} = F_1(x, y) + \sqrt{2D}\eta(t), \tag{3}$$

$$\frac{dx}{dt} = F_2(x, y) + \sqrt{2D}\eta(t), \tag{4}$$

in which the definitions of F_1 and F_2 are the same as those in the previous section. From the point of view of dynamics, this is a set of overdamped Langevin equations. D is the constant and isotropic diffusion coefficient, meaning the off-diagonal elements of diffusion matrix D, D_12, and D_21 are zero. $\eta(t)$ is the standard Gaussian white noise, $\langle \eta(t)\eta(t') \rangle = \delta(t-t')$, which can be regarded as a Wiener process with a diffusion coefficient of 1. According to these definitions, the global kinetic property can be described by a Fokker-Planck (FP) equation derived from Eqs. (3) and (4) [46]:

$$\frac{\partial P(x, y, t)}{\partial t} = -\frac{\partial}{\partial x}(F_1 P) - \frac{\partial}{\partial y}(F_2 P) + D\left(\frac{\partial^2}{\partial x^2} + \frac{\partial^2}{\partial y^2}\right)p. \tag{5}$$

The FP equation shows how our nonequilibrium system's state points distribute in phase space by probability, but what we are more interested in is the motion of the system in steady state. Equation (5) can be transformed into

$$\frac{\partial P(x, y, t)}{\partial t} = -\nabla \cdot \boldsymbol{J}, \tag{6}$$

in which $J_1 = F_1P - D(\partial p/\partial x)$ and $J_2 = F_2P - D(\partial P/\partial y)$. At the long-time limit, our nonequilibrium system reaches steady state, $\partial p/\partial t = -\nabla \cdot \boldsymbol{J} = 0$. The divergent free steady state probabilistic flux is rotational, which means $\boldsymbol{J}$ does not have to vanish and can be expressed as

$$\boldsymbol{J}_{ss} = \boldsymbol{F}P_{ss} - \boldsymbol{D} \cdot \nabla P_{ss}. \tag{7}$$

As the steady state probability flux vector, $\boldsymbol{J}_{ss}$ can represent the state points' motion trend of the system in the nonequilibrium steady state (NESS). Therefore, dividing both sides by P_{ss}, one gets

$$\boldsymbol{F}' = \frac{\boldsymbol{J}_{ss}}{P_{ss}} = \boldsymbol{F} + \boldsymbol{D} \cdot \nabla \boldsymbol{U}, \tag{8}$$

in which $U = -\ln(P_{ss})$ is generalized potential, and $\boldsymbol{F}'$ is composed of the deterministic generalized driving force $\boldsymbol{F}$ and diffusion effect [51]. In our work shown in a later section, we use U as the potential landscape to reveal the structural changes of the system in NESS.

The deterministic dynamic mechanism of the system ensures that the trajectory from a certain starting point will concentrate in the range of a certain path without excessive deviation when the noise is not too large. That "certain path," because of the presence of noise in stochastic dynamics circumstances, may be a little different from that in deterministic dynamics. We used the stochastic path integral to determine a dominant path, which benefited our work [52–57]:

$$\int_{\text{for all paths } x(t)} \cdots \int p[\boldsymbol{q}(t)]\mathcal{D}\boldsymbol{q}(t), \tag{9}$$

in which $\mathcal{D}\boldsymbol{q}(t)$ is integral for all paths and $p[\boldsymbol{q}(t)]$ is the probability of path $\boldsymbol{q}(t)$ in phase space:

$$\begin{aligned} P[\boldsymbol{q}(t)] &= \exp\left(-\int_{t_a}^{t_b} \mathcal{L}[\dot{q}(t), q(t)]dt\right) \\ &= \exp\left[-\int_{t_a}^{t_b} dt\left(\frac{1}{4D}\{\dot{q}(t) - f[q(t)]\}^2 + \frac{1}{2}\frac{df[q(t)]}{dq(t)}\right)\right]. \end{aligned} \tag{10}$$

The $f[q(t)]$ is the deterministic driving force and $\mathcal{L}[q(t), \dot{q}(t)]$ is the Lagrangian of the system. Using the Euler-Lagrange equation, the dominant path can be derived [58]. Its general principle and detailed technique can be viewed in the SM [43].

Additionally, to ensure consistency, we mainly adopt the Eulerian approach to solve the SDE. The discrete Wiener process is approached by adding random numbers according to the distribution $\sqrt{2D\Delta t}N(0, 1)$ in every time step, in which Δt is the time interval in the computation and $N(0, 1)$ is the standard normal distribution.

In this work, simulations of the SDE with white noise give adequate results. However, the master equation may reach better results being closer to actual biosystems; it has the general form (provided that the state space is continuous) [46]

$$\frac{\partial}{\partial t}P(z, t|y, t') = \int [W(z|x, t)P(x, t|y, t') - W(x|z, t)P(z, t|y, t')]dx, \tag{11}$$

where W is the propensity function. It is a fact that a Fokker-Planck equation can always be approximated by a master equation, while the reverse situation is usually true under a relatively low noise, as what we study in this work [46,59–62]. Therefore, results given by master equations are exceptional comparisons with the SDE simulation. In our work, we employ the Gillespie algorithm (SSA) as a method to simulate master equations of our model, which has been proven as an efficient approach to the chemical master equation [63,64]. Also, see details in the SM [43].

III. RESULT AND DISCUSSION

A. Landscape and streamline plotting

From a micro point of view, phenomena, which appear in a system determined by equations with the form as in Eqs. (3) and (4), are the joint presentation of cooperation and competition between stochastic noise and deterministic generalized forces. In our work, the dynamic structure in phase space is reconstructed by noise, or so-called fluctuating force, resulting in a new physical state of the global system in phase space throughout the entire domain of k_2. In order to further study this property, we select a representative point in each of the three domains of k_2, which are, respectively, $k_2 = 0.12$, 0.15, and 0.17. Figures 4(a)–4(c) show the deterministic dynamics structure of them.

As we have defined in the previous section, landscapes and steady state probability fluxes on it depict the kinetic structure of the system. Noticeably, a large circle adhered to the unstable manifold emerges, which can never exist in the deterministic dynamics system (Fig. 5). It is not only because this phenomenon is completely the product of stochastic action, but more importantly, the large circle cannot exist according to the Bendixson-Dulac theorem if it is regarded as a limit cycle to some extent.

The streamline plotting can be used as the evidence of the conclusion of landscapes [Figs. 4(a1)–4(c1)]. For the situation $k_2 = 0.12$, the large circle including the stable node and the saddle constitutes all of the dynamics structure. This is because all of the state points in phase space will return to the stable node driven by the deterministic generalized force, and the white noise makes these state points cross the saddle with a certain probability. For the situation $k_2 = 0.15$, this complex system has two circles. One is the stable limit cycle we have already verified, and another is the large circle created by the noise. Obviously, a part of the limit cycle clings to the stable manifold [Fig. 4(b1)]. Because of this, the state points running on the limit cycle can easily cross the stable

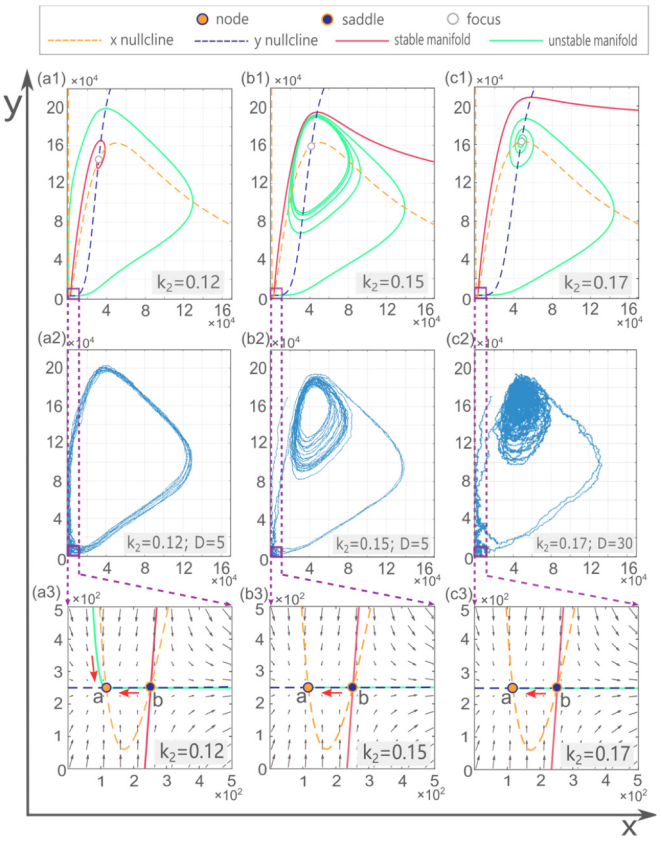

FIG. 4. Nullclines, stable and unstable manifolds, and deterministic forces in areas of the stable node and the saddle, of representative points in each of the three domains of k_2. (a1)–(c1) portray the deterministic dynamic structures. (a2)–(c2) depict stochastic streamlines, all the starting points of which are (1500, 17 500). Grid lines in (a1)–(c1) and (a2)–(c2) can assist the comparative observation. (a3)–(c3) are diagrams of deterministic forces and nullclines of the area where the stable node and saddle are, in which gray arrows depict deterministic forces and red arrows indicate the direction of unstable manifolds between saddles and stable nodes. Their subordinate relationships are marked by purple boxes and dashed arrows. Consistent with Fig. 2, "a" represents the stable node and "b" represents the saddle.

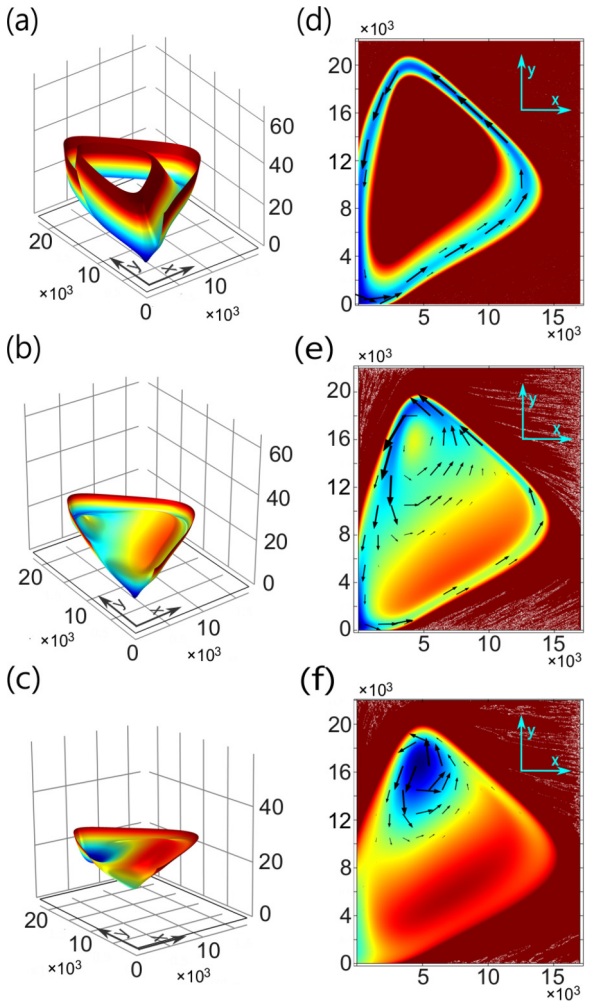

FIG. 5. Landscape and vertical view of $k_2 = 0.12$, 0.15, and 0.17. (a)–(c) are landscapes of $k_2 = 0.12$, 0.15, and 0.17 with $D = 5$, 5, and 30. The pruned parts are areas where the probabilities approach zero. (d)–(f) are vertical views of (a)–(c), in which the ranges of color change are the same as (a)–(d). The black arrows in vertical views show the $\boldsymbol{J}_{ss}$, the length being taken as the logarithm of the sizes of the flow at points where they are drawn. These arrows may not express the values of fluxes precisely, but they can be used to characterize where there are significant probability flows. More figures depicting the influence on the dynamic structures by changing D are in the SM [43].

manifold driven by noise (this is also one of the reasons why $k_2 = 0.15$ is chosen as the representative value). This means that the two circles may switch alternately. Besides, the larger the diffusion coefficient D is, the more the two circles mingle with each other, which is because the state points that have already jumped into the large circle have a higher probability of jumping back to the right side of the stable manifold before returning to the stable node. As for $k_2 = 0.17$, the stable manifold is far away from the unstable manifold, which resembles the classical bistable transition. Compared with the case of $k_2 = 0.12$ or 0.15, it is relatively difficult to form a large circle in this case. Therefore, we do not pay much attention to this situation, as long as we know that there are still transitions between two stable structures in the form of the large circle.

To clarify, the kinetic mechanism is of benefit to comprehend how the large circle, which is the main component of the quasiperiod to be discussed later, is produced. Generally, the deterministic force determines the global and large-scale motion tendency of the system. Meanwhile, fluctuations of the dynamic behavior of the system are generated by stochastic action. Namely, noise (random action term) makes the landscape change from the form with only deterministic force to the final form we get, and maintains the flow of $\boldsymbol{J}_{ss}$ together with deterministic force (Fig. 5). The emergence of the large circle does embody that. In the area on the right of the stable node and on the left of the saddle, deterministic forces, which are from right to left, are tiny, and stochastic action plays a predominant role [Figs. 4(a2)–4(c2)]. It makes state points prone to be driven from the vicinity of the stable node to the right of the saddle by the stochastic action, resembling a Brownian movement. The fluctuation at this special position

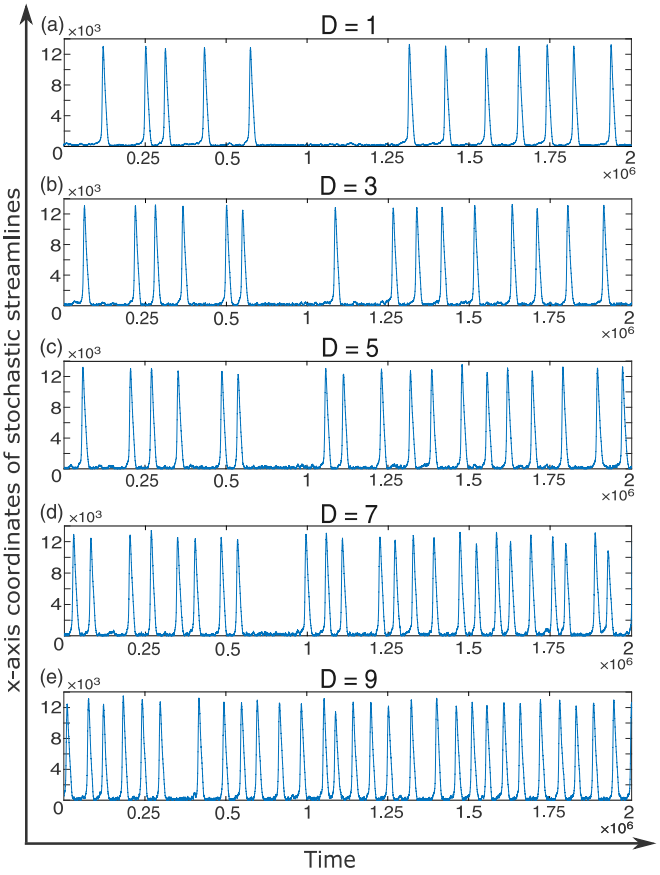

FIG. 6. Evolution of x-axis coordinates with time for $k_2 = 0.12$. Horizontal ordinates of (a)–(e) are x, and longitudinal coordinates of (a)–(e) are y. Since the dynamics of the system takes the form of oscillators, these diagrams look like amplitude diagrams. These graphs can be regarded as a supplement to the stochastic streamline plotting, which is convenient for us to observe the quasiperiodic behavior of the system. One can see the graph of a longer time range of 5×10^6 in the Appendix.

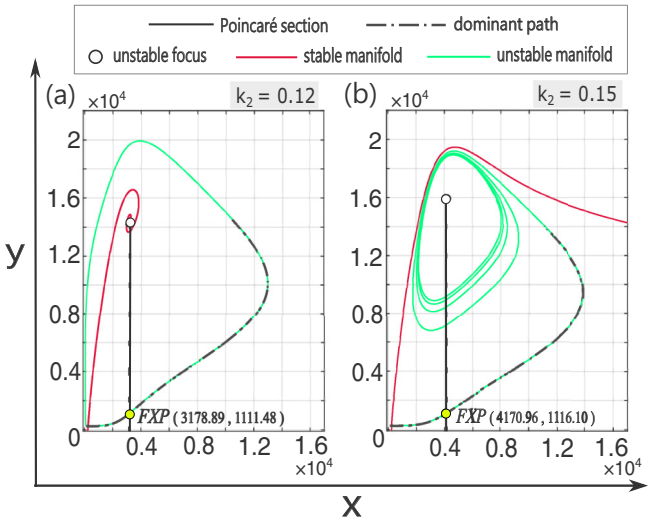

FIG. 7. Manifolds plotting and dominant paths. We select the situation $D = 5$ as examples. The black dashed lines are the dominant paths calculated by [Eq. (10)]. Because the dominant path integral will diverge in the region where the unstable manifold and the stable manifold are close to each other [this fact can also be seen in figures of landscapes, where the landscapes tend to be flat in this area (Fig. 5)], we truncate the total step length of the dominant path integral. Each dominant path starts from the stable node. For $k_2 = 0.12$, the stable node locates at (116.611, 250.002). For $k_2 = 0.15$, it is (116.611, 250.001). *FXP* is the intersection of the Poincaré section and the dominant path. For $k_2 = 0.12$, the unstable focus locates at (3178.89, 14 547.50). For $k_2 = 0.15$, it is (4170.96, 15 998.50).

performs the effect resembling a switch. After that, the state point is driven by the dominant deterministic force to form a large circle.

B. Barrier height, first passage time, and competing capacity of the quasiperiod

We will study the properties of the quasiperiod by analyzing two specific quantities, namely, mean first passage time (MFPT) and barrier height. It is advantageous to connect the two in series through a consistent definition, in which we want to define the first passage time as the time span that a state point moves from the stable node to a certain position on the right side of the saddle point. The reasons are sufficient: From Fig. 6, we can see that the widths of the thin and high peaks representing the large circle have no obvious change. Therefore, almost all the differences, which are between periods of large circles with different diffusion coefficients D, come from the expected time required to cross the barrier at the saddle from the vicinity of the stable node. Furthermore, only crossing the saddle does not guarantee that the state point will continue to move along with the unstable manifold and form the large circle. This can be learned from the streamline plotting and $t - x$ plotting, because the state point still has the possibility of returning to the left side of the saddle after crossing the saddle. This enlightens us that it is effective to introduce a Poincaré section at the appropriate position. In our work, starting from the unstable focus above, a straight line perpendicular to the x axis is the Poincaré section defined in this two-dimensional system, which is the "'certain position" (Fig. 7). In our work, the MFPT is calculated by directly averaging the first passage time obtained from 10 000 measurements.

Another problem is how to ensure that the state point under the effect of noise will cross the saddle and move along the unstable manifold with a certain probability, instead of diffusing to other areas. As we have mentioned earlier, calculating the dominant path by [Eq. (10)] is an efficient solution. As we see in Fig. 7, in the region where we are concerned and define the first passage time and barrier height, the dominant path almost coincides with the unstable manifold. When the total time steps are the same, the probability of the dominant path is much greater than that of other paths. This fact can also be seen by comparing [Figs. 4(a2)–4(c2)] with Fig. 7. Even if there is noise, the streamlines will not deviate from the dominant paths.

Naturally, we define the barrier height as follows: Barrier height $\Delta H = U_{FXP} - U_{\text{Fixed}}$. As the definition, the value of barrier height is the difference between the value of landscape U at *FXP* and that at the stable node. The definition of *FXP*

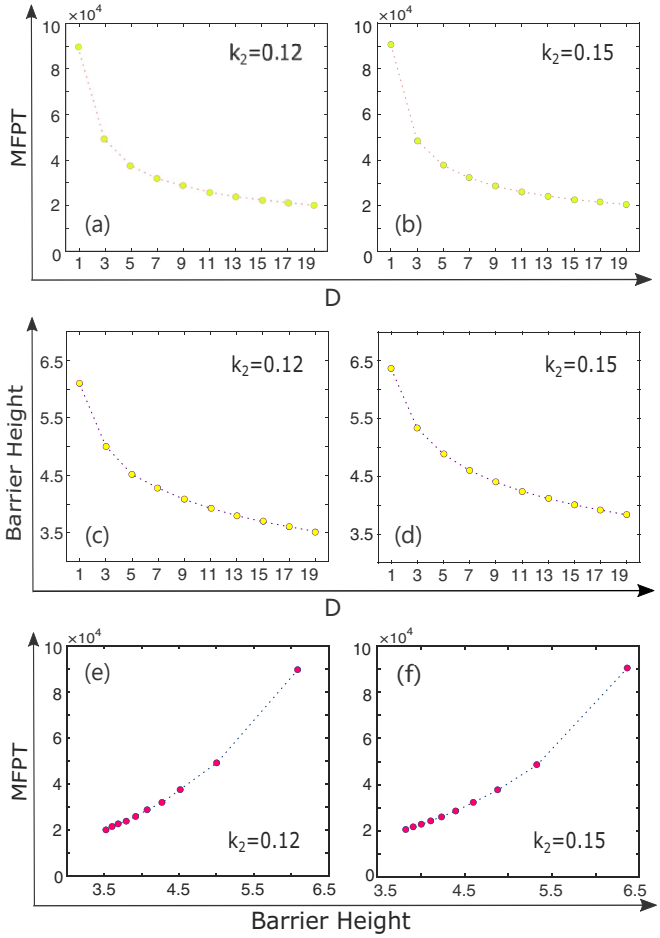

FIG. 8. (a), (b) Mean first passage time of $k_2 = 0.12$ and $k_2 = 0.15$. We confirm one measurement has been accomplished if the x-axis coordinate of the state point reaches the Poincaré section. (c), (d) Barrier height of $k_2 = 0.12$ and $k_2 = 0.15$. (e), (f) The relations between barrier height and MFPT.

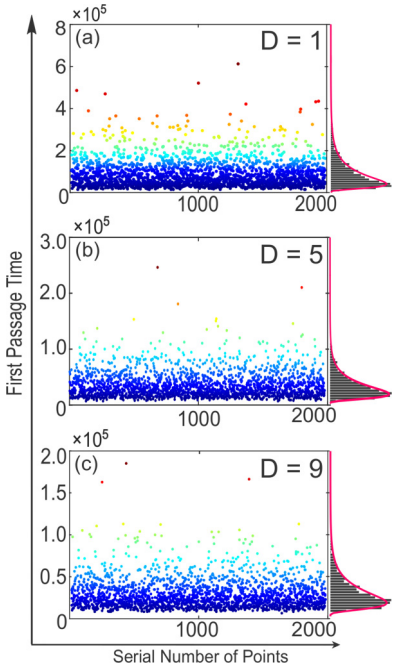

FIG. 9. Distributions of the first passage time with different diffusion coefficients D. For each D value, we record 2000 measurements. The fitting graph on the right side of each scatter diagram depicts the density distribution of points in the diagram, and its range is consistent with the ordinate of the scatter diagram. The inverse Gaussian distribution is used for fitting. The dark gray bar charts are proportions of the number of points in different intervals, and the magenta curves are fitting curves. Note that from (a) to (c), the range of each ordinate axis becomes smaller and smaller.

ensures the unity between barrier height and first passage time, which is convenient for us to investigate the relationship between them.

In Figs. 8(a) and 8(b), we have seen that with the diffusion coefficient D increasing, the MFPT decays rapidly and then tends to be stable and flat. This corresponds to Fig. 6; that is, the distance between peaks becomes closer with the diffusion coefficient D becoming larger and larger. In particular for $k = 0.12$, with the increase of the diffusion coefficient D, the appearance of the large ring will change from occasional pulse behavior to quasiperiodic behavior (Fig. 6). In the biological system we study, it implies an oscillator whose period is distributed in a certain range. Meanwhile, the data of barrier heights shown in Figs. 8(c) and 8(d) keep a high consistency with the MFPT.

Overviewing Figs. 8(a)–8(d), we can draw the following conclusions. First, the MFPT and the barrier height decrease monotonically with the increase of diffusion coefficient D. It is not difficult to understand that with the increase of the diffusion coefficient, the "activity" of the state point increases. In other words, the width of the expected value of the white noise composed by the Wiener process increases, which can cause appreciable effects. This is reflected in the landscapes, where the global shape flattens (Fig. 5). Second, with the increase of the diffusion coefficient D, the MFPT decays rapidly and then tends to be stable and flat. Observing the solution of a general Wiener process may help us to understand this fact that only when the diffusion coefficient D is small, will the shape of the function of the solution change significantly with the change of the diffusion coefficient D. Third, the polyline of barrier heights and the MFPT have similar shapes. In fact, there is also a monotonic relationship between the MFPT and the barrier height, in which the barrier height acts as a scale to measure the diffusion coefficient D [Figs. 8(e) and 8(f)]. This result is similar to that in Ref. [26].

Furthermore, the definition of the Poincaré section has another significant application, that is, to endow a justification for the quasiperiod constructed by the large circle (Fig. 9). $D = 1$, 5, and 9 are selected to reflect the evolution of distributions of the first passage time, which are fitted as inverse Gaussian which is always used to portray the distribution of Wiener processing with a positive drift. As mentioned earlier, this can be used as a characterization of the time of one cycle. On the one hand, one can see, respectively, that in Figs. 9(a)–9(c), distributions of each value of D are quite concentrated. On the other hand, following the increase of D, distributions become more and more concentrated, which is exhibited by the variety of lengths of longitudinal coordinates

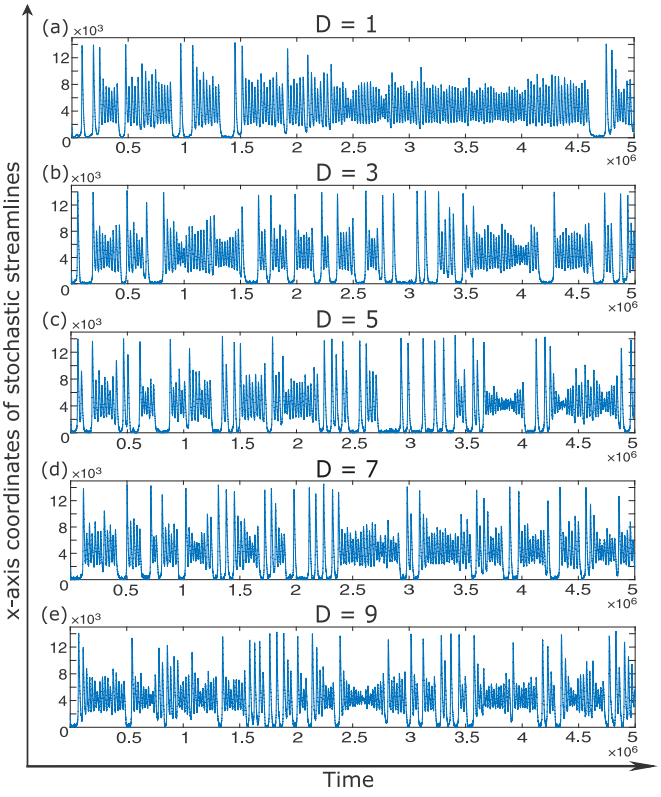

FIG. 10. Evolution of x-axis coordinates with time for $k_2 = 0.15$. Horizontal ordinates of (a)–(e) are x, and longitudinal coordinates of (a)–(e) are y.

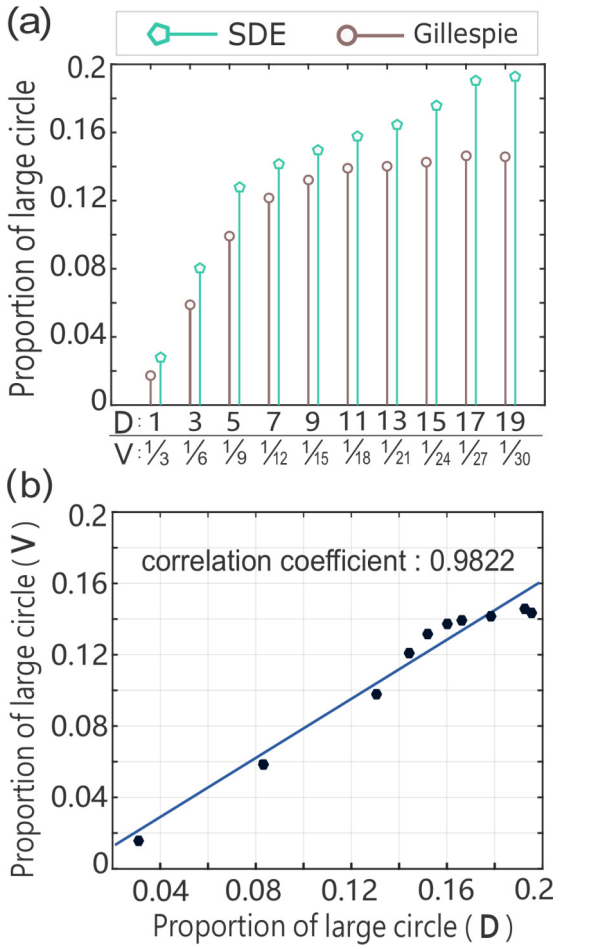

FIG. 11. (a) Proportions of large circles in whole dynamic processes of SDE simulation and SSA. (b) Results of linear correlation analysis between SDE simulation and SSA simulation. Each dark blue point is a one-to-one corresponding data point between SDE and SSA in (a). The light blue line is the linear fitting line.

being shorter and shorter. This means that not only for each D is the distribution of cycle length concentrated in a very limited region, but also the periodicity will become more and more stable with the increase of D. More information about the frequency can be found in the SM [43].

Figure 10 exhibits the competition between the large circle that is the quasiperiodic structure represented by high and thin peaks, and the original stable limit cycle that is the inherent periodic structure represented by relatively small oscillations. Here we use competition but not mixture to describe the situation of $k_2 = 0.15$ constructed by the large circle and the stable limit cycle together, because it is a dynamic process that with the increase of D, the occurrence frequency of the large circle rises obviously, as the large circle snatches the room originally belonging to the limit cycle. Interestingly, this competing capacity of the large circle has been implied in the case of $k_2 = 0.12$, in which the more intense the noise is, the more salient the quasiperiod is (Figs. 6, 9, and 15).

In Fig. 11(a) we concisely present a comparison between the Gillespie simulation algorithm (SSA) and the SDE simulation in the case of $k_2 = 0.15$, the comparison being about proportions of large circles in whole dynamic processes. These stemmed from $t - x$ data of the two simulation methods. If a peak is higher than 11 855, which is 85% of the maximum of the unstable manifold on the x coordinate, this peak will be regarded as representing a large circle. Parts of a large ring above 1391 are counted as the running time of the large ring, where 1391 is 10% of the maximum value of the unstable manifold. In addition, if a large circle is connected to a limit cycle, the connection will be cut off at 4171, which is the x coordinate of the unstable focus. Though there may be a situation where a circle, whose peak is higher than 13 909, does not pass across the barrier to be an intact dynamic process, it will still be considered as a large circle, because it indeed performs the function of the large circle. The parameters, $V = 1/3$, $1/6$, $1/9$, $1/12$, and $1/15$ in the Gillespie algorithm representing the intensity of stochasticity, correspond to $D = 1$, 3, 5, 7, and 9 in SDE simulation, respectively [62]. We can see that with the change of parameters, development trends of proportions of large circles are quite consistent. The capacity of large circles to compete with stable limit cycles in these processes becomes stronger and stronger, being reflected as proportions of large circles extend with the parameters' increase. Moreover, we did the linear correlation analysis between SDE simulation and SSA simulation [Fig. 11(b)]. The result is that there is a strong linear correlation between the two groups of data, which provides a considerable guarantee for the authenticity of SDE simulation.

C. Entropy production and heat dissipation

The well-known and widely used definition of entropy in the interdiscipline of statistical physics and derivative is as follows:

$$S = k_B \int_\Sigma P(x, y, t) \ln P(x, y, t) d\Sigma, \tag{12}$$

where k_B is the Boltzmann constant, and Σ is the domain of the system we studied. Thereupon, the time change rate of the entropy S is [39]

$$\begin{aligned} T\frac{\partial S}{\partial t} &= k_B \int_\Sigma (1 + \ln P)\nabla \cdot \boldsymbol{J} d\Sigma \\ &= -\int_\Sigma (k_B T \nabla \ln P - \boldsymbol{F}) \cdot \boldsymbol{J} d\Sigma - \int_\Sigma \boldsymbol{F} \cdot \boldsymbol{J} d\Sigma \\ &= \int_\Sigma \boldsymbol{\Pi} \cdot \boldsymbol{J} d\Sigma - \int_\Sigma \boldsymbol{F} \cdot \boldsymbol{J} d\Sigma \\ &= \mathrm{EPR} - \mathrm{HDR}. \end{aligned} \tag{13}$$

In Eq. (13), EPR is the entropy production rate, and HDR is the heat dissipation rate of which the original definition is the time derivative of the expected value of work done by deterministic generalized forces expressed in the form of the Stratonovich integral. The introduction of temperature T is to maintain thermodynamic consistency based on Einstein's relation $\boldsymbol{D}\boldsymbol{D}^T = 2k_B T$. Therefore, the thermodynamic force $\boldsymbol{\Pi} = \boldsymbol{F} + \boldsymbol{D} \cdot \nabla U$ [39,65]. If the system is in NESS, $\boldsymbol{\Pi} = \boldsymbol{J}_{ss}/P_{ss}$.

In NESS, we have

$$T\frac{\partial S}{\partial t} = \int_\Sigma (\boldsymbol{J}_{ss}/P_{ss} - \boldsymbol{F}) \cdot \boldsymbol{J}_{ss} d\Sigma = \int_\Sigma \boldsymbol{D}\nabla \boldsymbol{U} \cdot \boldsymbol{J}_{ss} d\Sigma = 0. \tag{14}$$

The most direct inference is that $\boldsymbol{J}_{ss}$ is orthogonal to ∇U. This can only be proved when $\boldsymbol{D} \to 0$ [66]. It can be explained vividly that the direction of $\boldsymbol{J}$ can be determined by the deterministic generalized force $\int_\Sigma \boldsymbol{F} \cdot \boldsymbol{J} d\Sigma dt$ only when the noise almost does not exist. The general explanation is that $\nabla \cdot \boldsymbol{J} = 0$, $\boldsymbol{J}$ is the curl flux, and the integral along any closed curve (i.e., the work done by ∇U) in the gradient field is zero.

Since the entropy production rate EPR is equal to the heat dissipation rate HDR in NESS, we only need to calculate the heat dissipation rate which is easy to calculate; then we can get all the information of the two. Figure 12 shows the heat dissipation rates of $k_2 = 0.12$ and $k_2 = 0.15$.

For $k_2 = 0.12$, the polyline of HDR is similar to that in other studies; it shows certain monotonicity and increases with the increase of the diffusion coefficient D [26,42]. Additionally, for $k_2 = 0.17$, the shape of the polyline is virtually identical to the result of $k_2 = 0.12$. For $k_2 = 0.15$, the polyline presents the shape of a check mark; it is not common that there is a minimum value of HDR in the neighborhood of $D = 3$. What is the essence of the entropy production rate and heat dissipation rate? What does the minimal value of the heat dissipation rate imply [Fig. 12(b)]? An intuitive illustration, which is that the increase of noise makes a part of $\boldsymbol{J}_{ss}$ shift from the stable limit cycle to the large circle, can be seen

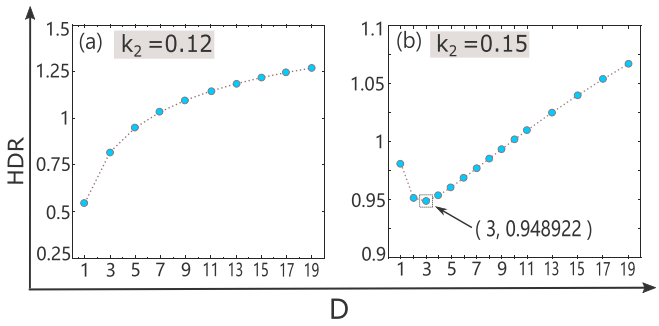

FIG. 12. Heat dissipation rates of $k_2 = 0.12$ and $k_2 = 0.15$. In (b), $k_2 = 0.15$, we reduce the interval between the points of diffusion coefficients D from 1 to 10, the reason for which is to make the minimal value of HDR more evident. In our calculation, $P(x, y, t)$ of each D has been normalized.

in the SM [43]. However, we prefer to clarify its physical significance in the following.

According to Eq. (8), we define $\boldsymbol{J} = \upsilon_p P(x, y, t)$, in which $\upsilon_p = \boldsymbol{F}'$ as the velocity of probability flow. Meanwhile, $\boldsymbol{F}$ from the overdamped Langevin equation is still interpreted as a generalized force. In the phase space dynamics determined by the FP equation and described by probability, the velocity of the state should be represented by υ_p. In this expression, $d\boldsymbol{x}/dt = u_p$. Therefore, the heat dissipation rate is

$$\mathrm{HDR} = \int_\Sigma \boldsymbol{F} \cdot \upsilon_p P d\Sigma. \tag{15}$$

Equation (15) has the form of power. It connotes that we may explicate HDR from the perspective of work. However, the self-consistency of this idea initiated by υ_p needs to be demonstrated before we continue to analyze it. One can see the proof in the SM [43].

The material derivative does not comprise the change of entropy produced by the motion of the state point (Eq. (S8) in the SM [43]), since in the whole process from the initial state to the nonequilibrium steady state, the deterministic generalized force $\boldsymbol{F}$ only plays the role of maintaining the movement of the state point. Its work is immediately dissipated by the overdamped system. From a global perspective, as a deterministic and constant force field, $\boldsymbol{F}$ pushes the dynamic point motion according to its established structure from beginning to end. $\boldsymbol{F}$ really consumes the energy supply of the system (in biological systems, the energy supply is chemical energy), which is reflected in the kinetic behavior of the system in the nonequilibrium state. This is the same whether it is in the NESS or before reaching the NESS.

On the contrary, the stable dynamic behavior of the system does not need to be continuously driven by the stochastic action $\boldsymbol{D}\nabla \boldsymbol{U}$, because the expected value of the diffusion motion driven by white noise is zero. Before reaching NESS, the result of its work is to make the state point reach the position where the deterministic force cannot be realized, which is the process of constructing the landscape (the dynamic structure of phase space) from the initial state. After reaching NESS, the development of the landscape has been completed, and the weighted average of $D\nabla U \cdot \upsilon_p$ is zero, which means that

the stochastic forces cancel each other, which is the character of thermal fluctuation.

In terms of probability, the deterministic force field is constant, which does not provide new possibilities for the state of the system. When the system reaches NESS, the landscape does not change, so the stochastic effect is zero. This is consistent with the explanation of entropy in statistical physics.

Through the above analysis, we know that heat dissipation is a measure of system energy consumption, which has the meaning of "power." This conclusion applies to all systems which can be described by Eqs. (3) and (4). For a biochemical system, such as a set of genetic circuits, the energetic material is generally ATP, and the stochastic effect comes from the hot bath, the randomness of biochemical reaction, or the copy noise of plasmids, and so on. For ecosystems, the energy supply materials may be producers and primary consumers, and the sources of noise are more extensive. No matter what kind of system, the explanation of Fig. 12(b) is the same: The minimum value of heat dissipation rate means that the system has a relatively minimum energy consumption rate; that is, the energy consumption required to maintain the system in NESS is the least.

D. Application to a practical model

Now we discuss a practical biological model. The model comes from [67]. Its main content can be described by equations similar to Eqs. (1) and (2):

$$\begin{aligned}\frac{dx}{dt} &= \upsilon + \frac{0.01gx^2}{r^2+0.01x^2} - \frac{0.1x}{1+0.1x+y},\\ \frac{dy}{dt} &= \frac{h}{1+10^{-5}k^5x^5} - \frac{y}{1+0.1x+y},\end{aligned} \tag{16}$$

where the parameters of this set of equations come from the supplemental material of [67]. $k = 4.5045$ is the coefficient of the regulating Hill function, which is normally an invariant. By adjusting coefficients g, h, r, and υ, one can obtain different dynamics structures of this model. We chose two sets of parameters to study. One set is $g = 0.043$, $h = 0.974$, $r = 0.3$, $\upsilon = 0.00028$. The system controlled by these parameters will be similar to the case in our work when $k_2 = 0.12$. That is, in the first quadrant, there are three fixed points in the system, which are stable node, saddle, and unstable focus [Fig. 13(a)]. Another set is $g = 0.106$, $h = 0.978$, $r = 0.4$, $\upsilon = 0.00016$. For equations controlled by this set of parameters, the system will present similarly to the case in our work of $k_2 = 0.17$. Three fixed points were found in the first quadrant, which are the stable node, saddle, and stable focus [Fig. 13(b)].

With the noise being introduced in this system, we can see in Fig. 13(c) that a large circle along with the unstable manifold is formed. It means that this actual biological system can also appear as noise-induced quasiperiodicity, and even switch between different periods by reasonably adjusting coefficients, i.e., reaction rates. To some degree, this shows that the quasiperiod induced by noise is common, and the results of our work are of general significance. Figure 14 shows the $t - x$ diagram of the situation of Figs. 13(a) and 13(c). It quite resembles Figs. 6 and 15.

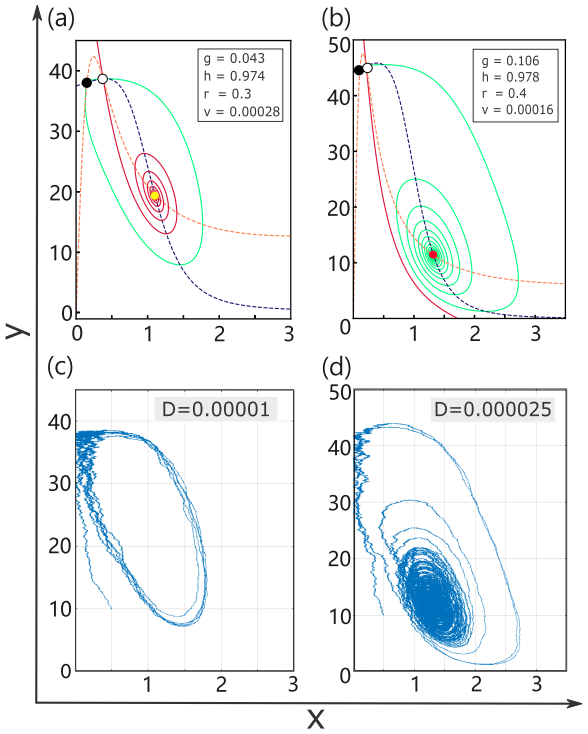

FIG. 13. Dynamics structures and stochastic streamlines of the model from [67]. The use of the color and line type is the same as Fig. 4. In (a), (b) at the top right corner, the black solid circle represents the stable node and the black hollow circle is for the saddle. In (a), the yellow solid circle represents the unstable focus. In (b), the red solid circle represents the stable focus. (c), (d) are stochastic streamline diagrams of the cases described in (a), (b), respectively.

Results of this practical model in this section consolidate the main content of our work: Noise can create a quasiperiod. It is absent in deterministic dynamics because there is a barrier constructed by the saddle and the stable node near each other, and stochastic action can push the state point to overcome the barrier. One thing is principal: As long as this *saddle-node-unstable focus* structure exists, we can expect the quasiperiodic behavior induced by noise. That is, the methods and results we have developed in our work are general.

IV. DISCUSSION

In this work, we utilized a classical model with positive and negative feedbacks, producing three kinds of dynamic structures by changing a key parameter k_2. We thoroughly studied two structures of them, one of which is the *saddle-node-unstable focus* structure that produced a quasiperiod by noise ($k_2 = 0.12$), and the other is the *node-limit cycle* structure that produced the switch between two quasiperiods by noise ($k_2 = 0.15$).

Now we can answer the questions raised at the beginning of this paper. Noise can induce the system to produce a new periodic state, which is different from the transition between bistable states or the relatively long stay near the unstable fixed point (similar to the case of $k_2 = 0.17$), and which is independent of the critical phenomenon near the bifurcation. In the case $k_2 = 0.12$, noise induces a quasiperiodic

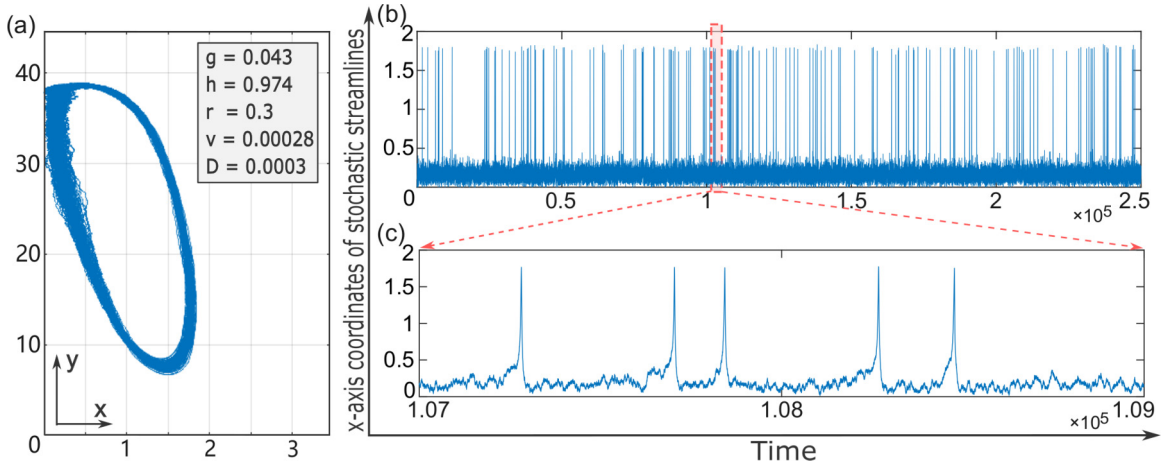

FIG. 14. The stochastic streamline and its $t - x$ diagram of the model discussed in this section, which is similar to the case in our work when $k_2 = 0.12$.

behavior resembling a *saddle node on an invariant cycle* (SNIC) bifurcation, which does not exist in the original system [68]. For $k_2 = 0.15$, the periodic behavior induced by noise coexists with the limit cycle in the original system and competes with each other, resembling a *saddle homoclinic orbit* (HOM) bifurcation based on an intrinsic stable limit cycle having existed [68]. This can only happen in a stochastic process.

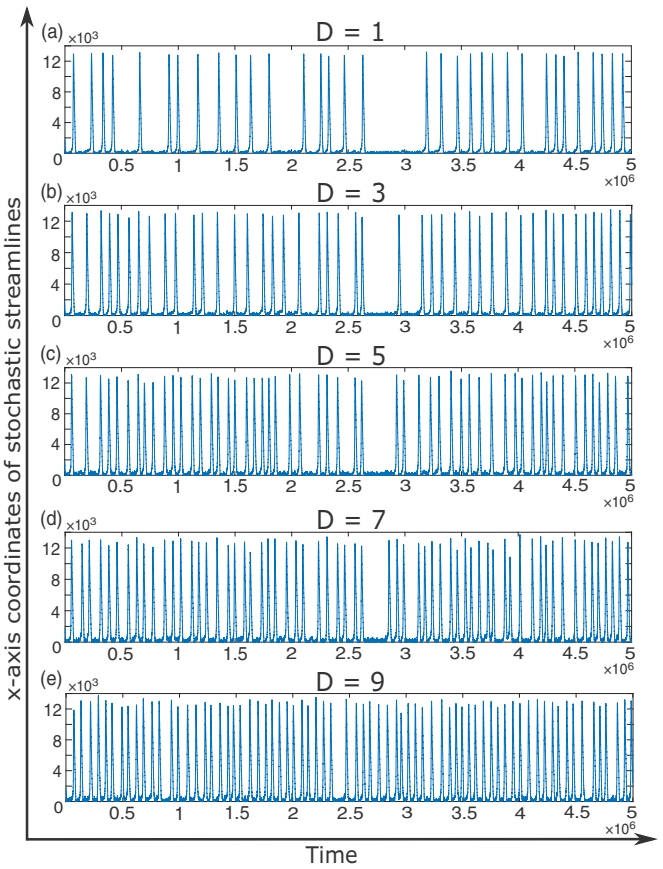

FIG. 15. Evolution of x-axis coordinates with time for $k_2 = 0.12$. Horizontal ordinates of (a)–(e) are x, and longitudinal coordinates of (a)–(e) are y. The time range is 5×10^6.

As long as the deterministic dynamic structure of a system has the *saddle-node-unstable focus* structure, the periodicity induced by noise has the conditions to realize, just as the biological example given in this work. In fact, similar genetic circuits can be synthesized artificially in synthetic biology [69–72]. By properly adjusting the rates of biochemical reactions, that is, the parameters in the differential equations, a structure that meets our requirements can be obtained.

For the case of $k_2 = 0.12$, the periodicity based on the large circle can be selectively activated by adjusting the noise intensity. The sensitivity of the system to noise can be realized by adjusting the distance between the saddle point and the node. If our research object is a biochemical system, such as the genetic circuit, this adjustment is to change some reaction rate. For $k_2 = 0.15$, it is worth noting not only the noise-induced large circle, but also the switch and competition between the two cycles. In particular, when the noise increases, the motion on the stable limit cycle becomes disordered, and the frequency of the large cycle increases. This may mean that in some systems, the large circle is an auxiliary mechanism to partly replace the unstable original periodic structure.

Period switch and competition are also reflected in nature. The periodical cicadas are a good instance [73,74]. There are many explanations about the life cycle of this insect, such as the seasonal cycle of the host [75], resource constraints [76], the influence of the ice age paleoclimate [77], and so on. Other work shows different views and mentions the mutation of the cycle [78]. Various reasons lead to periodical cicadas forming a set of accurate time counting mechanisms, and external factors such as climate, resources, and predators are the external factors that affect the timing mechanism, such as environmental noise. We might as well speculate that it may be a genetic circuit with unclear structure that controls the life cycle of the periodical cicadas. Thus, the case $k_2 = 0.15$ in our work is a potential approach to explain that.

In fact, the life cycle of 17-year cicadas is longer than that of 13-year cicadas by a 4-year inhibition period of early pupal growth. Reference [79] proved the homology between 13-year cicadas and 17-year cicadas by measuring the mitochondrial DNA of periodical cicadas, and this work negated the hybridization hypothesis, concluding that it is only

because 17-year cicadas experienced a rapid development period of 4 years in the development process. In terms of dynamics, if the extra 4 years are regarded as the time taken by the state point to cross a potential barrier, then a model similar to our work can be a candidate. Consequently, the case $k_2 = 0.12$ is an alternative, considering that the starting points of the cycle of 17-year or 13-year cicadas are, respectively, before or behind the barrier that reflects the rapid development period of 4 years. Another explanation is that the existence or absence of the barrier, respectively, represents the 17 or 13 years of cicadas. Details are in the SM [43].

In the model of this work, the constant α in $\boldsymbol{F}_1(x, y)$ represents the ratio of the formation rate of the molecule x to the degradation rate in the equation [Eq. (1)]. In other words, the process of α decreasing can be seen as the process where the ratio of "birth rate" to "death rate" of x gets smaller and smaller. In this way, as the ratio decreases, the original stable periodic structure diverges. The excessive attenuation of x caused by noise will result in the number of both x and y dropping to near zero rapidly. Then, a new cycle will be started stochastically, as described in Figs. S9(a), S9(b), S10(a), S10(b), S10(e), S10(f), S11(a), and S11(b) [43]. We expect that this will help to explain the dynamics of some species evolution.

It is expected that the results of this work can be verified in experiments and the real world. Further work should focus on whether it can set an effective switch to control the switching between two periods, or even turn on one period and turn off another. In addition, the significance of the minimum value of heat dissipation rate in the actual system is also worth exploring in the actual system.

APPENDIX

The parameters in Eqs. (1) and (2) were initially derived by a set of biochemical reactions, being the reaction rates. They may have been determined by experiment at that time, plus some artificial assumptions. No matter what, it hardly affects the result. In this work, parameters are

Equation (1): $\alpha_1 = 0.00875$, $\beta_1 = 7.5$, $k_1 = 2.5 \times 10^7$, $\delta = 4 \times 10^{-8}$, $\lambda_1 = 0.0004$, Hill coefficient $n = 2$.

Equation (2): $\alpha_2 = 0.025$, $\beta_2 = 2.5$, $\lambda_2 = 0.0004$, Hill coefficient $p = 5$; k_2 is the key parameter that changes according to the requirements.

These parameters are dimensionless in our work, which also reflects our original intention: We hope this work can benefit not only the genetic circuit, but also for broader research involving noise and periodicity.

[1] S. L. Harmer, S. Panda, and S. A. Kay, Molecular bases of circadian rhythms, Annu. Rev. Cell Dev. Biol. **17**, 215 (2001).

[2] M. J. Rust, J. S. Markson, W. S. Lane, D. S. Fisher, and E. K. O'Shea, Ordered phosphorylation governs oscillation of a three-protein circadian clock, Science **318**, 809 (2007).

[3] S. Yamaguchi, H. Isejima, T. Matsuo, R. Okura, K. Yagita, M. Kobayashi, and H. Okamura, Synchronization of cellular clocks in the suprachiasmatic nucleus, Science **302**, 1408 (2003).

[4] E. G. Biondi, S. J. Reisinger, J. M. Skerker, M. Arif, B. S. Perchuk, K. R. Ryan, and M. T. Laub, Regulation of the bacterial cell cycle by an integrated genetic circuit, Nature (London) **444**, 899 (2006).

[5] J. R. Pomerening, S. Y. Kim, and J. E. Ferrell, Jr., Systems-level dissection of the cell-cycle oscillator: Bypassing positive feedback produces damped oscillations, Cell **122**, 565 (2005).

[6] J. M. Raser and E. K. O'Shea, Control of stochasticity in eukaryotic gene expression, Science **304**, 1811 (2004).

[7] J. Paulsson, O. G. Berg, and M. Ehrenberg, Stochastic focusing: Fluctuation-enhanced sensitivity of intracellular regulation, Proc. Natl. Acad. Sci. USA **97**, 7148 (2000).

[8] E. M. Ozbudak, M. Thattai, I. Kurtser, A. D. Grossman, and A. van Oudenaarden, Regulation of noise in the expression of a single gene, Nat. Genet. **31**, 69 (2002).

[9] S. Cortijo and J. C. W. Locke, Does gene expression noise play a functional role in plants?, Trends Plant Sci. **25**, 1041 (2020).

[10] A. Eldar and M. B. Elowitz, Functional roles for noise in genetic circuits, Nature (London) **467**, 167 (2010).

[11] J. L. Cabrera Fernández, G. C. Herrera-Almarza, and E. D. Gutiérrez M., Chromosome progression and mitotic times behavior are mimicked by an stochastic unstable dynamics, Physica A (Amsterdam, Neth.) **512**, 1121 (2018).

[12] V. Kohar and M. Lu, Role of noise and parametric variation in the dynamics of gene regulatory circuits, npj Syst. Biol. Appl. **4**, 40 (2018).

[13] J. M. Pedraza and A. van Oudenaarden, Noise propagation in gene networks, Science **307**, 1965 (2005).

[14] G. M. Suel, R. P. Kulkarni, J. Dworkin, J. Garcia-Ojalvo, and M. B. Elowitz, Tunability and noise dependence in differentiation dynamics, Science **315**, 1716 (2007).

[15] J. M. G. Vilar, H. Y. Kueh, N. Barkai, and S. Leibler, Mechanisms of noise-resistance in genetic oscillators, Proc. Natl. Acad. Sci. USA **99**, 5988 (2002).

[16] G. K. Ackers, A. D. Johnson, and M. A. Shea, Quantitative model for gene regulation by lambda phage repressor, Proc. Natl. Acad. Sci. USA **79**, 1129 (1982).

[17] M. Assaf, E. Roberts, Z. Luthey-Schulten, and N. Goldenfeld, Extrinsic Noise Driven Phenotype Switching in a Self-Regulating Gene, Phys. Rev. Lett. **111**, 058102 (2013).

[18] J. Falk, M. Mendler, and B. Drossel, A minimal model of burst-noise induced bistability, PLoS One **12**, e0176410 (2017).

[19] T. B. Kepler and T. C. Elston, Stochasticity in transcriptional regulation: Origins, consequences, and mathematical representations, Biophys. J. **81**, 3116 (2001).

[20] M. Samoilov, S. Plyasunov, and A. P. Arkin, Stochastic amplification and signaling in enzymatic futile cycles through noise-induced bistability with oscillations, Proc. Natl. Acad. Sci. USA **102**, 2310 (2005).

[21] Y. C. Cheng and H. Qian, Stochastic limit-cycle oscillations of a nonlinear system under random perturbations, J. Stat. Phys. **182**, 47 (2021).

[22] M. Vellela and H. Qian, On the Poincaré-Hill cycle map of rotational random walk: Locating the stochastic limit cycle in a reversible Schnakenberg model, Proc. R. Soc. A **466**, 771 (2010).

[23] M. Turcotte, J. Garcia-Ojalvo, and G. M. Suel, A genetic timer through noise-induced stabilization of an unstable state, Proc. Natl. Acad. Sci. USA **105**, 15732 (2008).

[24] E. M. Ozbudak, A. Becskei, and A. van Oudenaarden, A system of counteracting feedback loops regulates Cdc42p activity during spontaneous cell polarization, Dev. Cell **9**, 565 (2005).

[25] J. Wang, Landscape and flux theory of non-equilibrium dynamical systems with application to biology, Adv. Phys. **64**, 1 (2015).

[26] J. Wang, L. Xu, and E. K. Wang, Potential landscape and flux framework of nonequilibrium networks: Robustness, dissipation, and coherence of biochemical oscillations, Proc. Natl. Acad. Sci. USA **105**, 12271 (2008).

[27] X. Fang, K. Kruse, T. Lu, and J. Wang, Nonequilibrium physics in biology, Rev. Mod. Phys. **91**, 045004 (2019).

[28] M. J. Klein and P. H. E. Meijer, Principle of minimum entropy production, Phys. Rev. **96**, 250 (1954).

[29] G. Nicolis and I. Prigogine, *Self-Organization in Nonequilibrium Systems* (Wiley, New York, 1977).

[30] D. Chaudhuri, Entropy production by active particles: Coupling of odd and even functions of velocity, Phys. Rev. E **94**, 032603 (2016).

[31] D. Mandal, K. Klymko, and M. R. DeWeese, Entropy Production and Fluctuation Theorems for Active Matter, Phys. Rev. Lett. **119**, 258001 (2017).

[32] K. Y. Wan and R. E. Goldstein, Time Irreversibility and Criticality in the Motility of a Flagellate Microorganism, Phys. Rev. Lett. **121**, 058103 (2018).

[33] F. Mura, G. Gradziuk, and C. P. Broedersz, Nonequilibrium Scaling Behavior in Driven Soft Biological Assemblies, Phys. Rev. Lett. **121**, 038002 (2018).

[34] F. Wong, A. Amir, and J. Gunawardena, Energy-speed-accuracy relation in complex networks for biological discrimination, Phys. Rev. E **98**, 012420 (2018).

[35] T. Ariga, M. Tomishige, and D. Mizuno, Nonequilibrium Energetics of Molecular Motor Kinesin, Phys. Rev. Lett. **121**, 218101 (2018).

[36] R. A. Blythe, Reversibility, Heat Dissipation, and the Importance of the Thermal Environment in Stochastic Models of Nonequilibrium Steady States, Phys. Rev. Lett. **100**, 010601 (2008).

[37] E. Lippiello, M. Baiesi, and A. Sarracino, Nonequilibrium Fluctuation-Dissipation Theorem and Heat Production, Phys. Rev. Lett. **112**, 140602 (2014).

[38] H. Qian, Nonequilibrium steady-state circulation and heat dissipation functional, Phys. Rev. E **64**, 022101 (2001).

[39] H. Qian, Mesoscopic nonequilibrium thermodynamics of single macromolecules and dynamic entropy-energy compensation, Phys. Rev. E **65**, 016102 (2001).

[40] B. Han and J. Wang, Quantifying robustness and dissipation cost of yeast cell cycle network: The funneled energy landscape perspectives, Biophys. J. **92**, 3755 (2007).

[41] B. Han and J. Wang, Least dissipation cost as a design principle for robustness and function of cellular networks, Phys. Rev. E **77**, 031922 (2008).

[42] S. Lapidus, B. Han, and J. Wang, Intrinsic noise, dissipation cost, and robustness of cellular networks: The underlying energy landscape of MAPK signal transduction, Proc. Natl. Acad. Sci. USA **105**, 6039 (2008).

[43] See Supplemental Material at http://link.aps.org/supplemental/10.1103/PhysRevE.105.014419 for more information about the content mentioned at the corresponding location in the text.

[44] S. Schecter, The saddle-node separatrix-loop bifurcation, SIAM J. Math. Anal. **18**, 1142 (1987).

[45] R. Thom, Topological models in biology, Topology **8**, 313 (1968).

[46] C. W. Gardiner, *Handbook of Stochastic Methods*, 3rd ed. (Springer, Berlin, 2004).

[47] N. Burić, K. Todorović, and N. Vasović, Influence of noise on dynamics of coupled bursters, Phys. Rev. E **75**, 067204 (2007).

[48] K. Pakdaman and S. Tanabe, Random dynamics of the Hodgkin-Huxley neuron model, Phys. Rev. E **64**, 050902(R) (2001).

[49] J. A. Reinoso, M. C. Torrent, and C. Masoller, Emergence of spike correlations in periodically forced excitable systems, Phys. Rev. E **94**, 032218 (2016).

[50] W. Yao, P. Yu, and C. Essex, Delayed stochastic differential model for quiet standing, Phys. Rev. E **63**, 021902 (2001).

[51] H. Feng and J. Wang, Potential and flux decomposition for dynamical systems and non-equilibrium thermodynamics: Curvature, gauge field, and generalized fluctuation-dissipation theorem, J. Chem. Phys. **135**, 234511 (2011).

[52] H. S. Wio, *Path Integrals for Stochastic Processes: An Introduction* (World Scientific, Singapore, 2013).

[53] M. Chaichian and A. Demichev, *Path Integrals in Physics. Volume I: Stochastic Processes and Quantum Mechanics* (Institute of Physics Publishing, London, 2001).

[54] J. Wang, K. Zhang, H. Lu, and E. Wang, Quantifying kinetic paths of protein folding, Biophys. J. **89**, 1612 (2005).

[55] R. Olender and R. Elber, Calculation of classical trajectories with a very large time step: Formalism and numerical examples, J. Chem. Phys. **105**, 9299 (1996).

[56] J. Wang, J. Onuchic, and P. Wolynes, Statistics of Kinetic Pathways on Biased Rough Energy Landscapes with Applications to Protein Folding, Phys. Rev. Lett. **76**, 4861 (1996).

[57] J. Wang, K. Zhang, H. Lu, and E. Wang, Dominant Kinetic Paths on Biomolecular Binding-Folding Energy Landscape, Phys. Rev. Lett. **96**, 168101 (2006).

[58] J. Wang, K. Zhang, and E. Wang, Kinetic paths, time scale, and underlying landscapes: A path integral framework to study global natures of nonequilibrium systems and networks, J. Chem. Phys. **133**, 125103 (2010).

[59] N. G. V. Kampen, *Stochastic Processes in Physics and Chemistry*, 3rd ed. (Elsevier, Amsterdam 2007).

[60] J. Keizer, *Statistical Thermodynamics of Nonequilibrium Proceses*, 1st ed. (Springer-Verlag, New York 1987).

[61] D. T. Gillespie, The chemical Langevin equation, J. Chem. Phys. **113**, 297 (2000).

[62] L. Xu, H. Shi, H. Feng, and J. Wang, The energy pump and the origin of the non-equilibrium flux of the dynamical systems and the networks, J. Chem. Phys. **136**, 165102 (2012).

[63] D. T. Gillespie, Exact stochastic simulation of coupled chemical reactions, J. Phys. Chem. **81**, 2340 (1977).

[64] D. T. Gillespie, A general method for numerically simulating the stochastic time evolution of coupled chemical reactions, J. Comput. Phys. **22**, 403 (1976).

[65] J. Schnakenberg, Network theory of microscopic and macroscopic behavior of master equation systems, Rev. Mod. Phys. **48**, 571 (1976).
[66] F. Zhang, L. Xu, K. Zhang, E. Wang, and J. Wang, The potential and flux landscape theory of evolution, J. Chem. Phys. **137**, 065102 (2012).
[67] G. M. Suel, J. Garcia-Ojalvo, L. M. Liberman, and M. B. Elowitz, An excitable gene regulatory circuit induces transient cellular differentiation, Nature (London) **440**, 545 (2006).
[68] J. Hesse, J.-H. Schleimer, and S. Schreiber, Qualitative changes in phase-response curve and synchronization at the saddle-node-loop bifurcation, Phys. Rev. E **95**, 052203 (2017).
[69] J. A. Brophy and C. A. Voigt, Principles of genetic circuit design, Nat. Methods **11**, 508 (2014).
[70] T. S. Gardner, C. R. Cantor, and J. J. Collins, Construction of a genetic toggle switch in *Escherichia coli*, Nature (London) **403**, 339 (2000).
[71] D. Sprinzak and M. B. Elowitz, Reconstruction of genetic circuits, Nature (London) **438**, 443 (2005).
[72] E. M. Judd, M. T. Laub, and H. H. McAdams, Toggles and oscillators: New genetic circuit designs, Bioessays **22**, 507 (2000).
[73] M. Lloyd and H. S. Dybas, The periodical cicada problem. I. Population ecology, Evolution: Int. J. Org. Evol. **20**, 133 (1966).
[74] M. Lloyd and H. S. Dybas, The periodical cicada problem. II. Evolution, Evolution: Int. J. Org. Evol. **20**, 466 (1966).
[75] R. Karban, C. A. Black, and S. A. Weinbaum, How 17-year cicadas keep track of time, Ecol. Lett. **3**, 253 (2000).
[76] L. H. Yang, Periodical cicadas as resource pulses in North American forests, Science **306**, 1565 (2004).
[77] H. Ito, S. Kakishima, T. Uehara, S. Morita, T. Koyama, T. Sota, J. R. Cooley, and J. Yoshimura, Evolution of periodicity in periodical cicadas, Sci. Rep. **5**, 14094 (2015).
[78] P. R. Grant, The priming of periodical cicada life cycles, Trends Ecol. Evol. **20**, 169 (2005).
[79] A. P. Martin and C. Simon, Anomalous distribution of nuclear and mitochondrial DNA markers in periodical cicadas, Nature (London) **336**, 237 (1988).